Conference on Modelling Fluid Flow (CMFF'15)
The 16th International Conference on Fluid Flow Technologies
Budapest, Hungary, September 1-4, 2015

ON THE SENSITIVITY OF PLANAR JETS

Péter Tamás NAGY[1], György PAÁL[2]

[1] Corresponding Author. Department of Hydrodynamic Systems, Budapest University of Technology and Economics. Műegyetem rkp. 3. D building 3rd floor, H-1111 Budapest, Hungary. Tel.: +36 1 463-1442, Fax: +36-1-463-30-91, E-mail: pnagy@hds.bme.hu
[2] Department of Hydrodynamic Systems, Budapest University of Technology and Economics. E-mail: paal@hds.bme.hu

ABSTRACT

Planar jets belong to the most researched flows. Many aspects of their instability have been well-known for a long while. One of them is the observation that the jet is more sensitive to disturbances near the orifice exit than elsewhere. Linear stability investigations on various velocity profiles were carried out using the Orr-Sommerfeld (OS) equation to find an explanation. The velocity profiles were provided by analytical approximations and numerical computational fluid dynamics (CFD) simulations.

A special method, the so-called compound matrix method (CMM) was used to solve the OS equation to provide sufficiently accurate results. The adaptation of the method for symmetric jets is derived briefly in this paper. The stability of different velocity profiles was compared based on the local spatial growth rate. The results of the comparison clearly show that velocity profiles near the orifice are more unstable than downstream ones. The local spatial growth rate of disturbance waves was higher close to the orifice. The reason for that was twofold, and these are explained in the paper.

Keywords: Compound matrix method, CMM, Orr-Sommerfeld equation, spatial stability investigation, symmetric planar jet

NOMENCLATURE

b_j	[-]	short notation in the compound matrix
i	[-]	the imaginary unit
n	[-]	arbitrary parameter to define velocity profile
x	[-]	dimensionless coordinate in the mean flow direction
$\hat{x}$	[-]	coordinate in the mean flow direction
y	[-]	dimensionless coordinate in the transversal direction
$\hat{y}$	[-]	coordinate in the mean flow transversal direction
$L(x)$	[m]	the local specific length
$U_{Max}(x)$	[m/s]	the local specific velocity
U_{Mean}	[m/s]	the global specific velocity
$U(y)$	[-]	the non-dimensional velocity profile
$\hat{U}(y)$	[m/s]	the velocity profile
$Re(x)$	[-]	the local Reynolds number
Re_{glob}	[-]	the global Reynolds number
Q	[-]	short notation for one of the characteristic roots of OS equation in the far field
α	[-]	the non-dimensional wavenumber
$\hat{\alpha}$	[rad/m]	the wavenumber
λ_j	[-]	the characteristic roots of OS equation in the far field
ω	[-]	the non-dimensional circular-frequency
$\hat{\omega}$	[rad/s]	the circular frequency
$\Phi(y)$	[-]	the non-dimensional amplitude of perturbation velocity
$\underline{\eta}(y)$	[-]	functions in CMM
$\underline{\tilde{\eta}}(y)$	[-]	the normalized functions in CMM

Subscripts and Superscripts

r	the real part of a variable
i	the imaginary part of a variable

1. INTRODUCTION

The Navier-Stokes equations have only a few analytical solutions. Several of these cannot be usually observed during experiments because they are unstable, as recognised by Reynolds. The stability investigations are still vital in fluid dynamics research.

The basic equation to describe the stability of parallel, incompressible flows is the Orr-Sommerfeld (OS) equation. In this paper planar jets

are investigated. The knowledge about their stability behaviour is essential to understand some phenomena (e. g. edge-tone) or even active flow control. It is assumed that the jet is infinitesimally disturbed at the nozzle, a disturbance wave starts, whose amplitude grows in the direction of the mean flow.

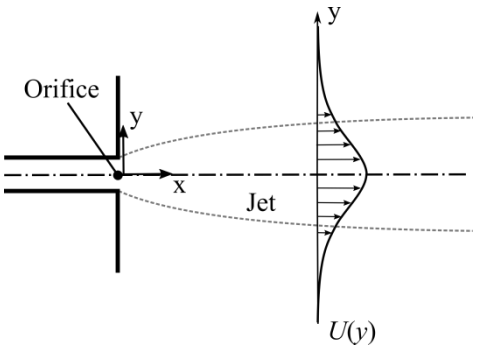

Figure 1. A jet with a (Bickley) velocity profile.

First Tatsumi, Kakutani [1] and Curle [2] investigated the planar jet. They used the OS equation to investigate the Bickley-profile which is the self-similar velocity profile valid far away from the nozzle. They determined the growth rate of disturbances at low Reynolds numbers (defined later) and the critical Reynolds number $Re_{crit} \approx 4$, below which the flow will be stable for any disturbance. Later Nolle [3] calculated the growth rate of disturbances for the same profile in an inviscid flow. The inviscid assumption means in the OS equation theoretically an infinite Reynolds number, practically a large enough number. He validated his calculations by experiments. At the same time Tam [4] investigated the same flow but for the non-parallel case. He stated that "the flow is unstable, regardless of Reynolds number, however defined."

Another observed phenomenon is that the jets are more sensitive to disturbances near the orifice exit [5], than elsewhere. The trivial explanation for this that if the growth of the disturbances is continuous in space then a disturbance which reaches the flow at the nozzle will be amplified along a longer path than the others. As far as the authors know, nobody investigated the growth rates close to the orifice. Only one paper was found [6] where the vicinity of the nozzle was studied. There the jet was modelled as a shear layer, which makes it difficult to compare the results near the orifice to the ones far away, where the Bickley-profile has already developed. The question asked in this paper is, why the jet is more sensitive to disturbances near the nozzle than elsewhere. We are providing an answer based on the stability investigation of various velocity profiles.

The stability investigation was performed using the OS equation in this paper, too. A special method, the so-called compound matrix method (CMM) [7] was used to solve the equation to provide accurate results. Another advantage of this method is that the boundary conditions at infinity can be prescribed simply. The adaptation of the method for symmetric flows is introduced briefly in Section 2. Two sets of velocity profiles were investigated: profiles given by analytical expressions and by CFD-simulations, which describe the flow at the orifice more precisely. They are treated in Section 3. In Section 4 the solution steps and the results of linear stability investigations are presented. Finally, in Section 5 we make some concluding remarks.

2. THE OS EQUATION AND THE COMPOUND MATRIX METHOD

2.1 The OS equation

The OS equation is a fundamental equation to investigate the stability of parallel, incompressible flows. It was derived from the continuity equation and the Navier-Stokes equations. The parallel flow assumption means that the velocity distribution does not change in the flow direction. This assumption is valid globally if the flow has solid, parallel boundaries (developed channel or pipe flow with parallel walls). In some other cases this assumption can be accepted as approximately valid if the flow is investigated locally, as in this paper. During the derivation non-linear terms are neglected and we look for the solution in a complex wave form leading to the well-known OS equation.

$$\Phi^{(iv)} - 2\alpha^2\Phi'' + \alpha^4\Phi = \\ \mathrm{i}\,Re\left\{(\alpha U - \omega)\left(\Phi'' - \alpha^2\Phi\right) - \alpha U''\Phi\right\}, \qquad (1)$$

where $\Phi(y)$ can be the amplitude of the dimensionless perturbation velocity or the amplitude of the stream function. In this paper the first one was used. $U(y)$ is the non-dimensional velocity profile in the equation. (The specific quantities for non-dimensionalization will be defined in Section 3.3) The dependence on the y variable was not denoted in many equations to keep them clear, but in the nomenclature it was denoted in every case. The definition of the parameters can also be found in the nomenclature.

If we take the limit of Eq. (1) at $Re \to \infty$ then the inviscid case can be obtained. This equation is known as the Rayleigh-equation (Eq. (2)) and it was solved for Bickley profile by Nolle [3].

$$(\alpha U - \omega)\left[\Phi'' - \alpha^2\Phi\right] - \alpha U''\Phi = 0 \qquad (2)$$

This equation was not used in this paper, but a comparison was made between Nolle's results and our large Reynolds number case.

2.2 The compound matrix method

Usually the solution of the OS equation leads to a boundary value and eigenvalue problem, because boundary conditions are prescribed at two locations. We have to find the α-ω parameter pairs, which fulfil the boundary conditions. Another problem is that this fourth order differential equation usually becomes stiff. Let us investigate the solution in the far field, at $y \to \infty$, where $U(y) = U''(y) = 0$ holds for jets. Here, the differential equation (Eq. (1)) can be simplified to (3).

$$\Phi^{iv} - 2\alpha^2\Phi'' + \alpha^4\Phi = \mathrm{i}\,Re\,\omega\left(\Phi'' - \alpha^2\Phi\right) \tag{3}$$

This equation has four different characteristic roots. $\lambda_{1,2} = \mp\alpha$ and $\lambda_{3,4} = \mp Q$ where $Q = \sqrt{\alpha^2 - \mathrm{i}\,Re\,\omega}$. For large Reynolds numbers $|\lambda_{3,4}| \gg |\lambda_{1,2}|$, which makes the problem stiff. One possibility to solve the problem is the compound matrix method (CMM), which is the best method according to Sengupta [8] for hydrodynamic problems. It provides accurate results and it can be easily implemented. This method was developed for the OS equation by Reid [7]. Later, Sengupta adapted this method for the Blasius profile, where some of the boundary conditions are prescribed at infinity, $y \to \infty$. In this paper his idea is followed during the adaptation of the method for symmetric plane jets.

The general solution of Eq. (1) can be written in the following form:

$$\Phi = a_1\Phi_1 + a_2\Phi_2 + a_3\Phi_3 + a_4\Phi_4 \tag{4}$$

where $\Phi_j(y)$ are the fundamental solutions and

$$\Phi_j(y) \propto e^{\lambda_j y} \text{ as } y \to \infty. \tag{5}$$

In the next step, the boundary conditions have to be prescribed at $y \to \infty$. The fluctuating velocities are assumed to be zero far from the jet, Eq. (6).

$$\Phi(y \to \infty) = \Phi'(y \to \infty) = 0 \tag{6}$$

This condition can be fulfilled only if the coefficients of the fundamental solutions, which grow exponentially for $y \to \infty$, have to be zero. This means $a_2(y) = a_4(y) \equiv 0$ because $\lambda_{2,4} > 0$.

Let us introduce six new functions (Eqs. (7) to (12)) and take the derivative with respect to y and substitute them to the OS equation (Eq. (1)) which leads to the differential equation system Eq. (13).

$$\eta_1 = \Phi_1\Phi_3' - \Phi_1'\Phi_3 \tag{7}$$

$$\eta_2 = \Phi_1\Phi_3'' - \Phi_1''\Phi_3 \tag{8}$$

$$\eta_3 = \Phi_1\Phi_3''' - \Phi_1'''\Phi_3 \tag{9}$$

$$\eta_4 = \Phi_1'\Phi_3'' - \Phi_1''\Phi_3' \tag{10}$$

$$\eta_5 = \Phi_1'\Phi_3''' - \Phi_1'''\Phi_3' \tag{11}$$

$$\eta_6 = \Phi_1''\Phi_3''' - \Phi_1'''\Phi_3'' \tag{12}$$

$$\underline{\eta}' = \begin{bmatrix} 0 & 1 & 0 & 0 & 0 & 0 \\ 0 & 0 & 1 & 1 & 0 & 0 \\ 0 & \mathrm{b}_1 & 0 & 0 & 1 & 0 \\ 0 & 0 & 0 & 0 & 1 & 0 \\ \mathrm{b}_2 & 0 & 0 & \mathrm{b}_1 & 0 & 1 \\ 0 & \mathrm{b}_2 & 0 & 0 & 0 & 0 \end{bmatrix} \underline{\eta} := \underline{\underline{A}}\underline{\eta}, \tag{13}$$

where $\mathrm{b}_1 := 2\alpha^2 + i\,\mathrm{Re}(\alpha\,\mathrm{U} - \omega)$ and $\mathrm{b}_2 := \alpha^4 + \alpha^2 i\mathrm{Re}(\alpha\mathrm{U} - \omega) + i\alpha\mathrm{Re}\,\mathrm{U}''$. In this case all the new functions have the same exponential growth rate for $y \to \infty$ as shown in Eqs. (14) to (19).

$$\eta_{1,\infty} \sim (-Q + \alpha)e^{-(\alpha+Q)y} \tag{14}$$

$$\eta_{2,\infty} \sim \left(Q^2 + \alpha^2\right)e^{-(\alpha+Q)y} \tag{15}$$

$$\eta_{3,\infty} \sim \left(-Q^3 + \alpha^3\right)e^{-(\alpha+Q)y} \tag{16}$$

$$\eta_{4,\infty} \sim \left(-\alpha Q^2 + \alpha^2 Q\right)e^{-(\alpha+Q)y} \tag{17}$$

$$\eta_{5,\infty} \sim \left(-\alpha Q^3 + \alpha^3 Q\right)e^{-(\alpha+Q)y} \tag{18}$$

$$\eta_{6,\infty} \sim \left(-\alpha^2 Q^3 + \alpha^3 Q^2\right)e^{-(\alpha+Q)y} \tag{19}$$

Let us normalize the $\underline{\eta}$ functions with the limit of the first one as $y \to \infty$ (Eq.(20)). In this case we get the limit at $y \to \infty$ for the normalized function (Eq. (21)), which are the initial conditions at $y \to \infty$. The normalization of the functions modifies the matrix in the differential equation (Eq. (13)) into Eq. (22).

$$\underline{\tilde{\eta}} = \frac{\underline{\eta}}{\eta_{1,\infty}} = \frac{\underline{\eta}}{-Q + \alpha} e^{(\alpha+Q)y} \tag{20}$$

$$\underline{\tilde{\eta}}_\infty = \begin{bmatrix} 1 \\ -(\alpha+Q) \\ \alpha^2 + \alpha Q + Q^2 \\ \alpha Q \\ -\alpha Q(\alpha+Q) \\ \alpha^2 Q^2 \end{bmatrix} \tag{21}$$

$$\underline{\tilde{\eta}} = [\underline{\underline{A}} + (\alpha+Q)\underline{\underline{I}}]\underline{\tilde{\eta}} \tag{22}$$

If we solve the differential equation system (Eq. (22)) with the initial conditions Eq. (21), it means

that the boundary conditions are automatically fulfilled in the far field. Since a fourth order differential equation needs four boundary conditions, the definition of two other boundary conditions is still necessary. For jets two choices are available. The first one is that assuming the perturbation velocity is zero in the far field on the other side of the jet, Eq. (23).

$$\Phi\left(y \to -\infty\right) = \Phi'\left(y \to -\infty\right) = 0 \qquad (23)$$

These boundary conditions can also be implemented, but if we use the symmetry boundary condition the computation cost can be halved. This means the amplitude of perturbation velocity is symmetric to the symmetry line of the jet, Eq. (24). (In the literature this condition is usually called antisymmetric, because the displacement of the jet is antisymmetric.)

$$\Phi'(0) = \Phi'''(0) = 0\,. \qquad (24)$$

Substituting Eq. (4) into Eq. (24) leads to Eqs. (25) to (26). This new linear equation system has a non-trivial solution if and only if the determinant of the associated matrix of the system of equations is zero (Eq. (27)). Eq. (27) is identical to the fifth component of $\underline{\eta}$ being 0 at y = 0 (Eq. (28)).

$$a_1\Phi_1'(0) + a_3\Phi_3'(0) = 0 \qquad (25)$$

$$a_1\Phi_1''(0) + a_3\Phi_3''(0) = 0 \qquad (26)$$

$$(\Phi_1'''\Phi_3' + \Phi_1'\Phi_3''')_{y=0} = 0 \qquad (27)$$

$$\eta_5(0) = 0 \text{ and } \tilde{\eta}_5(0) = 0 \qquad (28)$$

The original problem is simplified to an initial value problem, Eq. (22) should be solved with the initial condition Eq. (21) and choose the parameter pairs which fulfil Eq. (28). If these parameters are determined, the eigenvalue problem is solved and the eigenfunctions can be calculated. The original Φ function can be calculated in four different ways, we choose the one (Eq. (29)) presented in [8].

$$\eta_1\Phi'' - \eta_2\Phi' - \eta_4\Phi = 0 \qquad (29)$$

3. ANALYTICAL AND NUMERICAL VELOCITY PROFILES

3.1. Analytical velocity profiles

Schlicting in 1936 [9] and Bickley [10] in 1937 derived a velocity profile for a plane jet if a constant, line momentum source and self-similar flow is assumed. This velocity profile is a good approximation for jets far from the orifice. According to Nolle's experiments [3] this profile can be observed from 8 times the orifice size downstream. The Bickley profile in non-dimensional form is given in Eq (30).

$$U = \mathrm{sech}^2(y) \qquad (30)$$

Two special velocity profiles can be distinguished close to the orifice. The parabolic profile is developed if the nozzle is a long, parallel channel. The other one is "top-hat" profile, in which the boundary layer in the nozzle is very thin. In this case the nozzle is a short, convergent channel. An analytical approximation for the developing velocity profiles is available only in the case of "top-hat" outflow in [3] (Eq. (31)). The velocity profiles, which are closer to the orifice, can be defined by larger n parameters. In this paper the n = {1, 2, 3} cases were investigated, where n = 1 is identical to the original Bickley profile.

$$U = \mathrm{sech}^2(y^n) \qquad (31)$$

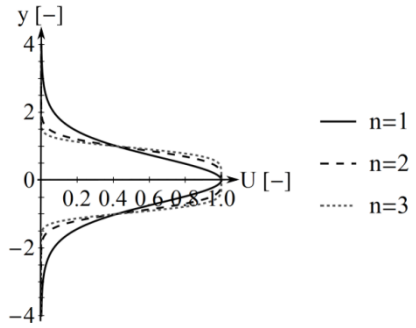

Figure 2. The analytical approximations of the velocity profile close to the orifice ($U = \mathrm{sech}^2(y^n)$).

Table 1. The comparison of the dimensionless flow rates between analytic profiles

Profile	Dimensionless flowrate [-]	The difference from Bickley-p. [%]
Bickley	2	0
$\mathrm{sech}^2(y^2)$	1.9056	-4.7
$\mathrm{sech}^2(y^3)$	1.9138	-4.3
"Top-hat"	2	0

The non-dimensional flowrates were calculated as a basis for the comparison. The result can be seen in Table 1. The maximum difference compared to the Bickley profile was less than 5 %.

3.2. The numerical velocity profiles

It was necessary to carry out CFD simulations because in the case of parabolic velocity profile there are no analytical formulae for the transition profiles between the parabolic and the Bickley profile. In the case of top-hat profile *n* can take only

whole numbers and the transitional profiles between cannot be produced analytically. The CFD simulations were carried out on a fine, structured mesh by ANSYS CFX. The size of the orifice was δ = 1 mm, the cell-size was 0.05 mm in the investigated domain, which was 24 mm long. The simulation was carried out at Re_{glob}=100. Re_{glob} is the global Reynolds number in the flow defined by Eq. (32).

$$Re_{glob} = \frac{\delta U_{Mean}}{\nu_{air}} \tag{32}$$

where ν_{air} = $1.545 \cdot 10^{-5}$ m^2/s is the kinematic viscosity of air at 25 °C and U_{Mean} = 1.545 m/s is the mean velocity at the orifice, which can be calculated based on the previous parameters. The global Reynolds number describes the whole flow. In contrast, the local Reynolds number belongs to a given cross-section and describes the local velocity profile. To be consistent with analytical profiles the specific quantities for the local Reynolds number were defined by Eq. (33) as $U_{Max}(\hat{x})$ is maximum velocity in a certain cross-section, $L(\hat{x})$ is the width where the velocity is equal to $0.42 \cdot U_{Max}$, coming from the evaluation of Bickley profile at y=1 since $sech^2(1) \approx 0.42$. In this case all the previously defined analytical and numerical profiles are non-dimensionalized on the same way ($1^n = 1$).

$$Re = \frac{L\, U_{Max}}{\nu_{air}} \tag{33}$$

The further non-dimensional quantities were calculated by Eqs (34) to (35).

$$\alpha = \hat{\alpha} L \tag{34}$$

$$\omega = \hat{\omega} \frac{L}{U_{Max}} \tag{35}$$

where $\hat{\square}$ denotes the quantity with dimensions.

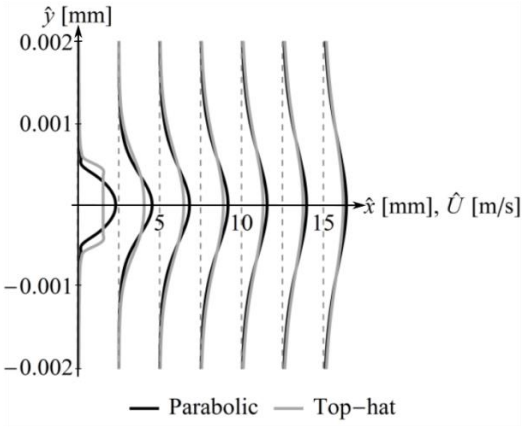

Figure 3. The velocity profiles at various distances from the orifice.

The velocity profiles are exported from CFX at various distances, shown in Figure 3.

The OS equation was used in a non-dimensional form, so that the velocity profiles had to be transformed into the same form. The transformed dimensionless velocity profiles can be seen in Figure 4, where the Bickley profile was also plotted. The velocity profiles turned more rapidly into Bickley profile in the case of parabolic outflow compared to the "top-hat" outflow. The Bickley profile was developed in both cases when $\hat{x} \gtrsim$ 6-8 mm, as it was noted experimentally by Nolle [3], too. Here, the usage of non-dimensional profiles highlights its advantage. If $\hat{x}$ > 8 mm, the stability results for non-dimensional Bickley profile can be used after redimensionalization. If the dimensional form of the stability equations had been be used, the whole solution procedure of the OS equation should have been repeated instead of a simple redimensionalization.

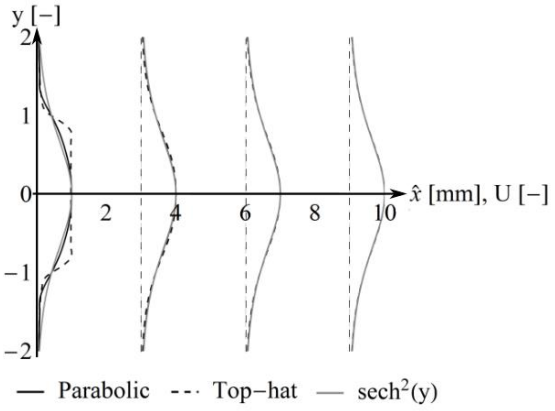

Figure 4. The dimensionless velocity profiles at various distances from the orifice.

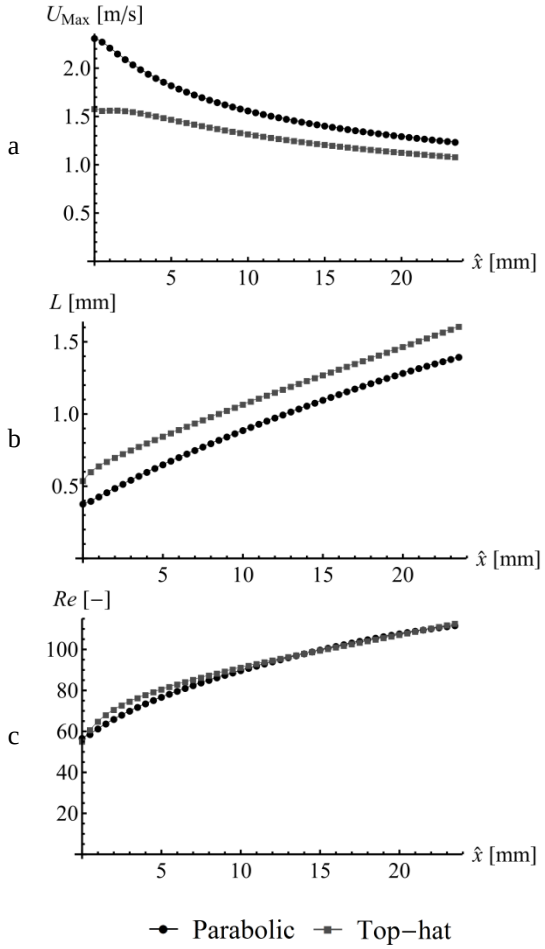

Figure 5. The velocity (a) and the length (b) scales and the local Reynolds number along the mean flow direction ($\hat{x}$).

The various scales were also plotted along the mean flow direction in Figure 5. The following observation can be made based on Figs. 4 to 6 for the dimensional velocity profiles. Although the transformations to the Bickley-profile were rapid in both case, the two flows with different outflows at the orifice (parabolic, "top-hat") are not identical even far from the nozzle. The maximum velocity is always a bit higher in the parabolic case (**a**), while the width of the jet is always a bit larger (**b**) in the "top-hat" case. The continuous increase of the local Reynolds number (**c**) is also observable, which was theoretically also derived far from the orifice [11].

4. THE SOLUTION METHOD AND THE RESULTS

4.1. The solution method

The following parameters should be determined or calculated in the Orr-Sommerfeld equation. The first one is the Reynolds number that could be a specified value (in a real flow, numerical velocity profiles) or an arbitrary parameter (in general, analytic velocity profile). The task is to determine the remaining two parameters, the wave number (α) and circular frequency (ω), which fulfil the condition in Eq. (28). These pairs are the solutions of the eigenvalue problem. Let us define the function D(Re, U, ω, α) (Eq. (36)) then we have to find the roots of this function (D=0).

$$\mathrm{D}\left(Re,\ U, \omega,\ \alpha\right) := \eta_5(y=0)\,|_{Re,U,\omega,\ \alpha} \qquad (36)$$

In the general case the wave both α and ω can be a complex number, but this means innumerable solutions. Here, the spatial stability analysis was used, the amplitude of the wave grows only in space, $\alpha = \alpha_r + \alpha_i$ is a complex number, while ω is real. The spatial growth rate is $\mu_s = -\alpha_i$. In experiments it is possible that the amplitude of the disturbance wave grows both in space and time, but comparison with experiments shows very good agreement with spatial stability analysisin the case of planar jets.

The initial condition Eq. (21) for the differential equation system Eq. (22) is prescribed at $y \to \infty$. A sufficiently large y value has to be chosen such that the boundary conditions are approximately fulfilled and Eq. (5) is true. In the case of analytical profiles y = 12 was chosen where $\mathrm{sech}^2(12) \approx 10^{-10}$. In the case of numerical profiles the velocity in the far field is never zero because of numerical errors. Here a spatial window function, which is one at the centreline of the jet and zero far away from it, was used to avoid this problem. In this case the "infinity" was chosen as the width of the function: y = 4.

The critical point during the solution procedure is to determine the first eigenvalue pair. Here, we followed the idea of Sengupta [12]. In the first step the Reynolds number was fixed to 100 in the case of analytic profiles and to the calculated Reynolds number in the case numerical profiles. ω was also fixed at 0.1 in both cases. A fine grid was made in the α-plane $\alpha_r \in [0,2]$ and $\alpha_i \in [-2,1]$ and the differential equation was solved for each α parameter on the grid. The investigation on a larger area is not necessary because a lower α_i means very rapid amplification, which is not observed experimentally. At the same time positive values mean decaying waves that are not interesting from our point of view. After that the $\Re\mathrm{e}(\eta_5(0))=0$ and $\Im\mathrm{m}(\eta_5(0))=0$ contour lines were plotted and the intersection point of these lines is detected. These points are the eigenvalues corresponding to different modes and they are sorted according to ascending α_i values, because lower values mean more rapid growth. It can be assumed that if the Re and ω parameters are changed slightly, the corresponding α values change only slightly. After one point is determined the next point was calculated by modifying slightly the parameters and using the Newton-Raphson method for which the initial guess was the previous solution. With this technique all eigenvalue pairs can be determined for

one mode starting from one known intersection point in the α plane. In this paper only the first mode was investigated.

4.2. Results

4.2.1 Results for the analytic profiles

Our results for Bickley the profile are compared to those of Nolle [3] to verify our calculations, for high Reynolds number. The comparison at various Reynolds number can be seen in Figure 6. At Re = 1000 our results were almost identical to the results of Nolle that means the stability properties of the Bickley profile above this number are independent of the Reynolds number.

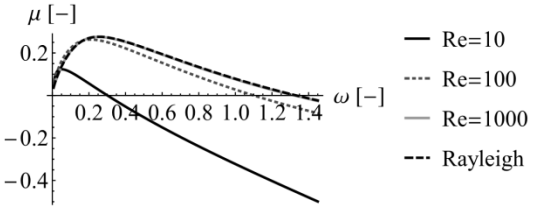

Figure 6. The growth rate of the amplitude of perturbation velocity in the case of Bickley profile for various Reynolds numbers and in the inviscid case (Rayleigh).

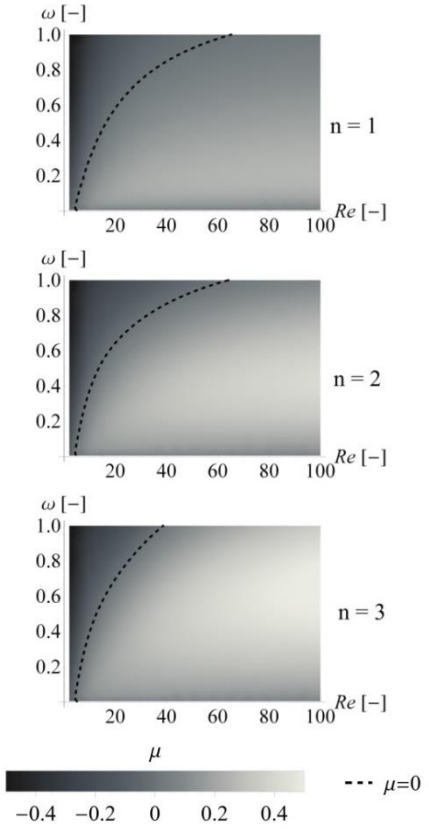

Figure 7. The growth rate of the amplitude of perturbation velocity for various *ω*, *Re* parameters in the case of analytic profiles ($U = \mathrm{sech}^2(y^n)$).

If we reduce the Reynolds number, the non-dimensional growth rate also decreases. The critical Reynolds below which the growth rate is always negative (the perturbation decays) and the flow is stable, is $Re_{crit} \approx 4.3$. This number was also predicted to be 4.0 in [1] and [2]. This number was the same for all analytic profiles for any n = {1 ,2, 3} parameters, as shown also in Figure 7. There the dashed line means the neutral stability curve, where the growth rate of perturbation is zero. Another observation is the lower branch of neutral stability curve tends so rapidly to the $\omega = 0$ axis in all cases that it is not visioble in Fig. 7, as calculated in [1] and [2] for the Bickley profile only.

Beside the similarities there is significant difference between the results of the analytical profiles. At a given Reynolds number the growth rates were much higher for large n parameters except at low frequencies. This can be seen in Figure 8. These results show us that the growth of the perturbation velocity wave is more rapid close to the orifice (for large n).

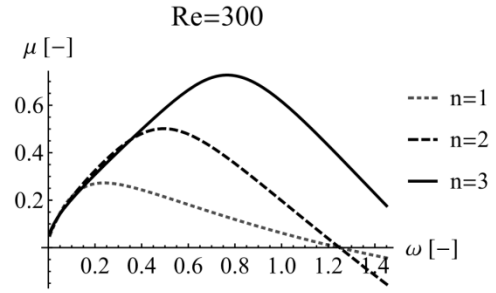

Figure 8. The growth rate of the amplitude of perturbation velocity at *Re* = 300 in the case of analytic profiles ($U = \mathrm{sech}^2(y^n)$)

4.2.2 Results for the numerical profiles

The results were the same in the case of numerical profiles. In Figure 9. the non-dimensional growth rates were plotted at various distances. The growth rates were higher for velocity profiles which are closer to the orifice, except at low frequencies.

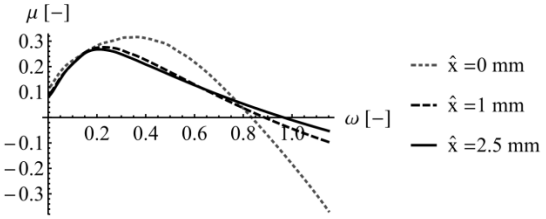

Figure 9. The non-dimensional growth rate of the amplitude of perturbation velocity in the case of numeric profiles at various distances from the orifice.

The non-dimensional results were redimensionalized. The redimensionalized growth-rates were plotted as a function of circular frequency in Figure 10. In this case the differences

were more significant, because the local width changes magnify the differences. The dimensional growth rate is inversely proportional to the length scale (Eq. (34)) which is the smaller closer to the orifice than far from it.

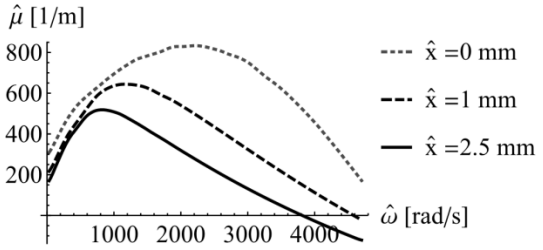

Figure 10. The growth rate of the amplitude of the perturbation velocity in the case of numerical profiles at various distances from the orifice

CONCLUSIONS

In this paper linear stability investigations of various velocity profiles were carried out by the OS equation solved by the CMM. The main goal of the investigation was to give an explanation why the flow at the orifice is more sensitive than elsewhere. The stability results showed that the disturbances grow more rapidly closer to the orifice. These observations were valid to analytical velocity profiles as well as for numerical profiles obtained from CFD. In the case of analytical velocity profiles the critical Reynolds number was the same in all cases $Re_{\text{crit}} \approx 4.3$ and the non-dimensional growth rate is virtually independent of *Re* if $Re \gtrsim 1000$.

The reason for the higher growth rate close to the orifice was twofold. The first reason was that the velocity profiles, that are closer to the top hat profile, have higher non-dimensional spatial growth rates. These profiles are closer to the orifice. The other one can be explained by the non-dimensional form of stability equations. The local length scale grows continuously from the orifice and the growth rate is inversely proportional to the local length scale for the same non-dimensional velocity profile.

REFERENCES

[1] Tatsumi, T. and Kakutani T., 1958, "The stability of a two-dimensional laminar jet," *J. Fluid Mech.*, vol. 4, no. 3, pp. 261-275.

[2] Curle, N., 1957, "On Hydrodynamic Stability in Unlimited Fields of Viscous Flow," *Proceedings of the Royal Society of London*, vol. 238, no. 1215.

[3] Nolle, A. W., 1998,"Sinuous instability of a planar air jet: Propagation parameters and acoustic excitation," *Acoustical Society of America*, pp. 3690-3705.

[4] Tam, K. K., 1955, "Linear stability of the non-parallel Bickley jet," *Canadian Applied Mathematics Quarterly*, vol. 3, no. 1.

[5] Kerschen, E. J., 1966, "Receptivity theory in compressible flow jet control" AFOSR program final report, Ft. Belvoir Defense Technical Information Center.

[6] Parekh, D. E.; Cain A. B., and Vaporean C: N., 1997, Characterization of Receptivity in jet flow control, UNITED STATES AIR FORCE Air Force Office of Scientific Research

[7] Sengupta, T. K., 2012, *Instabilities of Flows and Transition to Turbulence*, CRC Press.

[8] NG, B. S. and Reid, W. H., 1978, "An initial value method for Eigenvalue Problems Using Compound Matrices," *Journal of Computational Physics*, vol. Physics 30, pp. 125-136.

[9] Schlichting H., 1933, "Laminare Strahlausbreitung," Z. *Angew. Math. Mech.*, vol. 13, pp. 260-263.

[10] Bickley, W., 1937, "The plane jet," *Philos. Mag.*, vol. 23, pp. 727-731, 1937.

[11] White, F. M., 1991, *Viscous fluid flow*, McGraw-Hill.

[12] Sengupta, T. K.; Ballav M. and Nijhawan S., 1994, "Generation of Tollmien-Schlichting waves by harmonic excitation," *Phys. Fluids*, vol. 6, no. 3, pp. 1213-1222.